Photochemical Chlorination of Graphene

Bo Li,† Lin Zhou,† Di Wu,† Hailin Peng,† Kai Yan, Yu Zhou, and Zhongfan Liu*

Center for Nanochemistry, Beijing National Laboratory for Molecular Sciences (BNLMS), State Key Laboratory for Structural Chemistry of Unstable and Stable Species, College of Chemistry and Molecular Engineering, Peking University, Beijing 100871, People's Republic of China. †These authors contributed equally to this work

ABSTRACT We report the covalent functionalization of graphene by photochemical chlorination. The gas-phase photochlorination of graphene, followed by the structural transformation of the C—C bonds from sp^2 to sp^3 configuration, could remove the conducting π-bands and open up a band gap in graphene. X-ray photoelectron spectroscopy revealed that chlorine is grafted to the basal plane of graphene, with about 8 atom % chlorine coverage. Raman spectroscopy, atomic force microscopy, and transmission electron microscopy all indicated that the photochlorinated graphene is homogeneous and nondestructive. The resistance increases over 4 orders of magnitude and a band gap appears upon photochlorination, confirmed by electrical measurements. Moreover, localized photochlorination of graphene can facilitate chemical patterning, which may offer a feasible approach to the realization of all-graphene circuits.

KEYWORDS: graphene · covalent functionalization · photochemical chlorination · band gap opening

Since the first isolation of free-standing graphene,[1] a single-layer of sp^2-bonded carbon atoms, this two-dimensional crystal has been receiving much attention as a novel electronic material owing to its unique band structure and physical properties.[2−5] Although pristine graphene is one of the most chemically inert materials, graphene chemistry—the chemical modification of graphene to create derivatives with different structures and tunable properties—presents an exciting new direction in both theoretical and experimental research.[6−12] In particular, band gap engineering of graphene through chemical modification such as hydrogenation,[8] fluorination,[9−11] and organic functionalization[13] is appealing for electronics applications since it facilitates the scalable fabrication of graphene-based devices without breaking their resilient C—C bonds. However, novel and facile approaches for the covalent modification of graphene to tailor its electronic, optical, and chemical properties are still highly desirable.[14]

In the present work, we demonstrate a photochemical chlorination of graphene through the covalent attachment of chlorine radicals to the basal carbon atoms of graphene. This is a totally new approach for the functionalization and band structure engineering of carbon nanomaterials. After photochlorination, the addition of chlorine to the conjugated structure of graphene, followed by the structural transformation of the C—C bonds from sp^2 to sp^3 configuration, is sufficiently confirmed by comprehensive characterizations such as micro-Raman, atomic force microscopy (AFM), X-ray photoelectron spectroscopy (XPS), transmission electron microscopy (TEM), UV—vis spectroscopy, and electrical measurements. The resistance was found to increase over 4 orders of magnitude, and a band gap appeared. The nondestructive, homogeneous, and patternable photochlorination of graphene may open new possibilities for future electronic devices.

RESULTS AND DISCUSSION

Figure 1a illustrates the present route to produce photochlorinated graphene. A xenon lamp radiation causes chlorine molecules to split into highly reactive chlorine radicals, which presumably combine with graphene by a free radical addition reaction. Two kinds of starting materials were used: graphene flakes mechanically exfoliated from Kish graphite[15] and graphene films grown by chemical vapor deposition (CVD).[16−19] To avoid precontamination of foreign Cl species, the CVD-grown graphene film was detached by etching the copper away with a $Fe_2(SO_4)_3$ aqueous solution rather than $FeCl_3$. The graphene samples were transferred to oxidized silicon substrates (300 nm thick SiO_2) and subsequently annealed up to 370 °C in forming gas (50% Ar/50% H_2) to further remove residues.[20] Single- and few-layer graphene samples were identified *via* optical microscopy and subsequently confirmed by micro-Raman spectroscopy and AFM.[21,22] The photochemical reactions were performed for various reaction times in a home-built gas-phase photochlorination

* Address correspondence to zfliu@pku.edu.cn.

Received for review May 11, 2011 and accepted June 9, 2011.

Published online June 09, 2011
10.1021/nn201731t

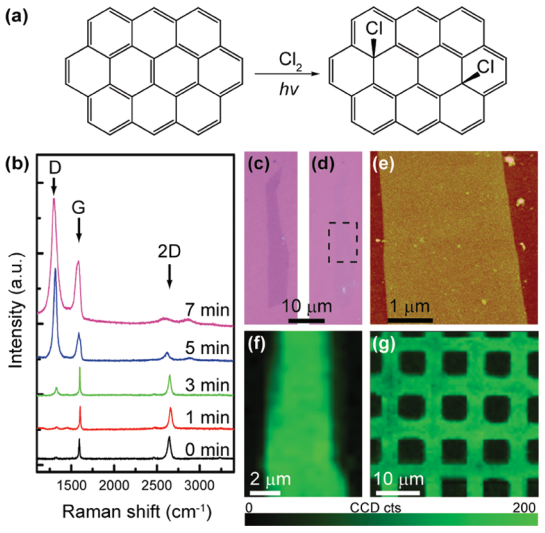

Figure 1. (a) Scheme of the photochemical chlorination process. (b) Raman spectra (wavelength λ_{ex} = 632.8 nm) evolution for single-layer graphene reacted with chlorine under xenon lamp irradiation. (c, d) Optical images of a single-layer graphene sheet before and after photochemical chlorination, respectively. (e) Typical AFM image of the same photochlorinated graphene sample with a *z*-scale of 10 nm. (f) D band mapping (λ_{ex} = 514.5 nm) for the photochlorinated single-layer graphene over the dashed box area in (d). (g) D band mapping for a CVD-grown graphene film after a patterned photochlorination.

system [see Figure S1 in the Supporting Information (SI)] at room temperature under a chlorine/nitrogen mixture pressure of 1 atm. A xenon lamp with maximum power density of 1.4 W/cm^2 was used to initiate the reaction. The effective wavelength is 320−620 nm, which was proved to be innocuous to graphene in the absence of chlorine.

Figure 1b shows the time evolution of Raman spectra for a single-layer graphene sample after a series of photochlorination reactions. As the photochlorination time increases, the characteristic disorder-induced D band at 1330 cm^{-1} emerges. In addition, the double-resonance 2D band around 2654 cm^{-1} significantly weakens, while the G band around 1587 cm^{-1} broadens due to the presence of a defect-induced D′ shoulder peak at 1620 cm^{-1}.[22] These observations strongly suggest that covalent C−Cl bonds were formed and thus a high degree of structural disorder was generated by the transformation from sp^2 to sp^3 configuration. Indeed, after 10 min of photochlorination the Raman spectra look more like that of graphene oxide or highly disordered carbon-based materials.[23] The Raman signature of the graphene is almost completely suppressed after 15 min of reaction. This indicates that the sp^2-bonded carbon network of graphene might be broken into nanoflakes (Figure S2 in SI). In contrast, control experiments without xenon lamp irradiation do not show an analogous chlorination phenomenon (Figure S3 in SI). Note that a clear difference between single-layer and bilayer graphene in the photochlorination reaction has been observed (Figure S4 in SI), similar to the case for photochemical reaction between graphene and benzoyl peroxide.[14] Interestingly, optical contrast of the single-layer graphene became more transparent upon photochlorination (Figure 1c,d). The enhanced transparency of chlorinated graphene was further confirmed by ultraviolet−visible (UV−vis) absorption spectroscopy (Figure S5 in SI), suggesting a band gap opened in the graphene's electronic spectrum.[9−11] An AFM image of the same sample revealed that the transparent chlorinated graphene is not etched upon photochlorination. The height of the chlorinated graphene monolayer is in the range 1.1−1.7 nm, slightly larger than average height (∼0.9 nm) of the pristine graphene (Figure 1e and Figure S6 in SI).

Micro-Raman mapping was performed to evaluate the uniformity of photochlorination. The intensity map of the D band (1250 to 1450 cm^{-1}) for the chlorinated graphene monolayer (Figure 1f) shows uniformly distributed color, indicating the high homogeneity of photochlorination within the spatial resolution of the Raman instrument (∼1 μm). The homogeneous photochlorination facilitates the chemical patterning of graphene films using a chlorine-resistant mask. Here, Al/Ti pads served as the mask to protect the graphene against photochlorination (Figure S7 in SI) and were then released by hydrochloric acid. The Raman D band intensity map reveals that the exposed region was efficiently photochlorinated while the masked regions remained intact, where the masked regions would be used for conductive pathways of all-graphene devices (Figure 1g).

XPS was performed to determine the composition and bonding type of the photochlorinated graphene (Figure S8 in SI). Figure 2a,b shows high-resolution XPS scans for Cl 2p and C 1s peaks of the photochlorinated graphene film, respectively. The prominent Cl 2p peaks at 200.6 eV ($2p_{3/2}$) and 202.2 eV ($2p_{1/2}$) are assigned to C−Cl bonds, unequivocally indicating the covalent bond formation between Cl and graphene. The XPS C 1s peak can be fitted with three different peaks with binding energy at 284.8, 286.6, and 289.0 eV, assigned to C−C, C−Cl, and O−C═O bonds, respectively.[24] The surface coverage of C−Cl groups was estimated by taking the ratio of the C−Cl peak area in Cl 2p to the C peak area in C 1s after considering the atomic sensitivity factors for Cl 2p and C 1s. The coverage is approximately 8 atom % (*ca.* 20.5 wt %) for this sample.

Structural information about the photochlorinated graphene film was obtained with TEM and selected area electron diffraction (SAED). The free-standing photochlorinated graphene film was carefully transferred onto a Cu grid and was recognized under low magnification with a sufficient defocus (Figure 2c). High-resolution TEM images show a homogeneous and featureless membrane (Figure 2d). Energy-dispersive

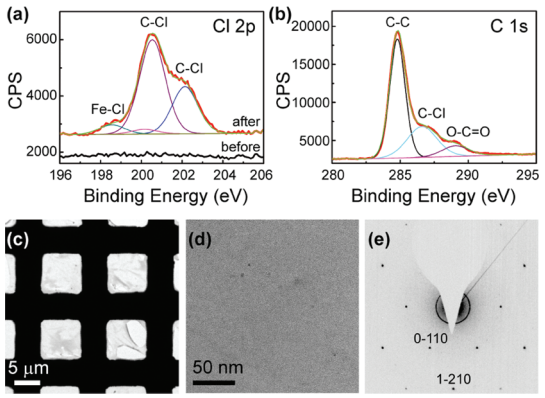

Figure 2. (a) High-resolution XPS Cl 2p spectra of the CVD-grown graphene film before (black) and after photochlorination (red). The weak $FeCl_3$ peaks at 198.6 and 200.2 eV were observed, presumably owing to the reaction of chlorine with the Fe ion residues from the $Fe_2(SO_4)_3$ etchant. (b) XPS spectra of C 1s in the same photochlorinated graphene. The peak of the O−C═O bond may be attributed to the presence of carbon oxide contaminations. (c) Low-resolution TEM image of photochlorinated graphene supported by a copper grid. (d) High-resolution TEM image of chlorinated graphene. (e) Corresponding selected area electron diffraction (SAED) pattern.

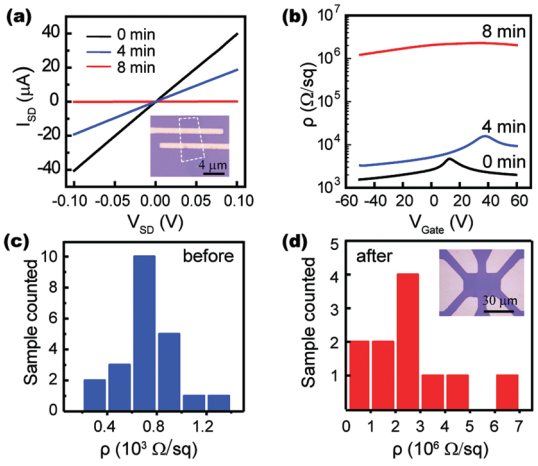

Figure 3. (a) Source−drain current (I_{SD}) *vs* voltage (V_{SD}) characteristics of three graphene FET devices under different degrees of photochlorination. Inset is a typical optical image of a graphene device after reaction. (b) Sheet resistance *vs* gate voltage curve for typical graphene devices with different reaction time. The carrier mobility is about 5000, 1400, and 1 $cm^2\ V^{-1}\ s^{-1}$ for the pristine graphene, 4 min photochlorinated graphene, and 8 min photochlorinated graphene, respectively. (c) Sheet resistance distribution of pristine graphene devices measured by the standard four-probe method. (d) Sheet resistance distribution of the photochlorinated graphene samples. Inset is the optical image of a four-probe graphene device.

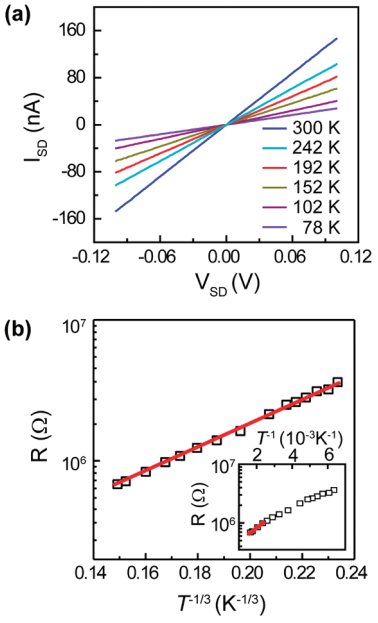

Figure 4. (a) Source−drain current (I_{SD}) *vs* voltage (V_{SD}) characteristics of the sample photochlorinated for 8 min at selected temperatures. From top to bottom: T = 300, 242, 192,152, 102, and 78 K. (b) Semilog plot of the resistance R *vs* $T^{-1/3}$ of the sample in (a). Inset: Semilog plot of R *vs* T^{-1}.

X-ray spectroscopy (EDX) equipped in the TEM was used to reveal the chemical composition of the photochlorinated graphene films. Within the accuracy of EDX analyses (∼1−2%), the Cl signal was clearly detected in the EDX spectra, although the Cl peak is much smaller than the dominant C peak (Figure S9 in SI), in agreement with the XPS results. Extensive SAED studies reveal that most regions of the photochlorinated graphene film generate a single set of hexagon diffraction patterns (Figure 2e), indicating the nondestructive nature of the domains.[8,25] Further investigations on the structural transformation process and detailed chlorination reaction mechanism are still desired.

Transport measurements were performed to study the electronic properties of chlorinated graphene. Both pristine and chlorinated graphene field-effect transistors were fabricated on Si/SiO_2 substrates using conventional electron beam lithography followed by metal (5 nm Cr and 45 nm Au) deposition. The transport measurements were carried out in a vacuum probe station (∼10^{-5} Torr). Figure 3a shows that the room-temperature resistance increased significantly with prolonged reaction time and increased 3 orders of magnitude after 8 min of photochlorination. Meanwhile, the carrier mobility decreased from ∼5000 $cm^2\ V^{-1}\ s^{-1}$ to ∼1 $cm^2\ V^{-1}s^{-1}$ (Figure 3b). Note that the contact resistance in the two-probe devices, as can be extracted by fitting the ambipolar curves,[26] was much less than the sample resistance. In addition, we have measured the resistance change upon photochlorination of more than 15 CVD-grown graphene devices with four-probe configuration (Figure 3c,d). The sheet resistance of the CVD-grown graphene samples increased almost 4 orders from ∼700 Ω/sq to ∼2 MΩ/sq upon 6 min photochlorination. The significant reduction of conductivity can be interpreted as the scenario where photochlorination may interrupt the conjugated system, reduce the charge in the conducting π-orbital, introduce scattering centers, or open up the band gap.

Variable-temperature electrical measurements in vacuum were further carried out to verify the semiconducting property of photochlorinated graphene. Unlike the semimetallic character of a pristine graphene with zero band gap, graphene after 8 min of photochlorination shows an obvious resistance increase by about an order of magnitude upon cooling from 300 K to 78 K (Figure 4a), suggesting a semiconductive behavior. Best linear fits of the temperature-dependent data were obtained by plotting $\ln(R)$ *vs* $T^{-1/3}$ (Figure 4b), indicating that variable range hopping (VRH) may be a plausible charge-transport mechanism in the chlorinated graphene. Such a mechanism is quite reasonable in our photochlorinated graphene samples, where nanoscale islands of graphene may remain as a result of the non-uniform addition of chlorine. The domain size might be small, below the spatial resolution limits of our Raman instrument and diffraction pattern studies. We also plotted R *vs* $1/T$ in a semilog plot (the inset of Figure 4b). The linear fit with the high-temperature (200 to 300 K) data may be described by the exponential T dependence $R \propto \exp(-\Delta/2k_BT)$. Extracted from the fit, the band gap $\Delta = 45$ meV. Due to the presence of localized states in the band gap, the expected band gap of chlorinated graphene should be much larger than the measured band gap of 45 meV, analogous to the disordered two-dimensional electron gas in silicon inversion layers[27] and fluorinated graphene.[28]

CONCLUSION

In summary, we developed a nondestructive, homogeneous, and patternable photochemical chlorination method to graft chlorine to the basal plane of graphene and fully characterized the photochlorinated graphene samples using micro-Raman, AFM, UV–vis spectroscopy, XPS, TEM, and electrical measurements. After photochlorination, the formation of C–Cl bonds with a coverage of up to 8 atom % was verified. The resistance was found to increase over 4 orders of magnitude, and a band gap appeared. The photochlorination of graphene could enrich and open up new possibilities for graphene-based electronic applications and may serve as a new platform for creating various functional derivatives through further chemical modification of the C–Cl bonds.

EXPERIMENTAL SECTION

Graphene Sample Preparation. The single-layer graphene films were grown on a copper surface using low-pressure CVD in a horizontal tube furnace using procedures analogous to those in published literature[16–18] and in our previous work.[19] The as-grown films are predominantly single-layer graphene, with a small percentage (less than 5%) of the area having few layers, owing to the self-limiting effect of Cu surface under low growth pressure.[16] Transferring graphene films from the Cu foil onto arbitrary substrates including SiO_2/Si was carried out. To avoid precontamination of foreign Cl species, the CVD-grown graphene film was detached by etching the copper away with a 2.0 mol/L $Fe_2(SO_4)_3$ aqueous solution rather than $FeCl_3$. After cleaning by dilute sulfuric acid and deionized water repetitively, the graphene supported by PMMA film was picked up by the chosen substrate. PMMA was removed by boiling acetone and subsequently annealed up to 370 °C in forming gas (50% Ar/50% H_2) to further remove residues.

Photochemical Chlorination. The photochemical reactions were performed in a home-built gas-phase photochlorination system that is composed of a quartz photoreactor, a chlorine generator, a desiccator, feed lines for gases, a tail-gas treatment unit, valves, and a pump (Figure S1 in SI). Chlorine gas is highly toxic and must be handled with great care. The photochemical chlorination system was placed and operated within a laboratory fume hood. Chlorine-resistant polytetrafluoroethylene tubing was used. Care was taken to ensure no detectable leak in the system by performing leak checks.

Graphene flakes on the Si/SiO_2 substrates were placed in the quartz photoreactor connected to the chlorine generator and desiccator. All experiments were performed under an atmosphere of dry nitrogen with the rigid exclusion of air and moisture by using standard Schlenk techniques. Chlorine gas was obtained by dropping 25 mL of hydrochloric acid (9 mol/L) into a three-necked flask that contained 5 g of MnO_2 at 90 °C. The chlorine gas was dried using concentrated sulfuric acid before entering the photoreactor. A xenon lamp (PLS-3SXE300, Trusttech) with a maximum power density of 1.4 W/cm^2 vertically irradiated the samples. An infrared transmitting reflector was used to decrease the thermal radiation effect.

Characterizations. AFM was carried out on a Vecco IIIa nanoscope using the tapping mode. Raman spectra were collected *via* a Renishaw system 1000 micro-Raman spectrometer with 632.8 nm excitation and a Horiba HR800 Raman system with 514.5 nm excitation. The laser spot size was about 1 μm. The laser power was kept at <1 mW/μm^2 to avoid a heating effect. Raman mapping was conducted by piezo-driving mirror scanning with a step size of 0.6–0.8 μm. The Raman integration time during mapping was 1 s. UV–vis spectra of photochlorinated graphene were recorded on a Perkin-Elmer Lambda 950 UV–vis spectrometer. XPS measurements were carried out using a Kratos Axis Ultra spectrometer with Al Kα monochromated X-ray at low pressures of 5×10^{-9} to 1×10^{-8} Torr. The large-area CVD-grown single-layer graphene films on Si/SiO_2 substrates were used for photochlorination and XPS characterization. The collection area was about 300×700 μm^2. The highest peak in C 1s spectra was shifted to 284.8 eV for charge correction. TEM of the photochlorinated graphene sample was studied by a 300 kV FET Tecnai F30 TEM apparatus. The photochlorinated graphene film was detached by etching the supporting SiO_2 substrate away with a dilute HF aqueous solution (~2 wt %) and subsequently transferred to a Cu TEM grid with the assistance of a spin-coated PMMA film. The PMMA film was then removed with acetone. Variable-temperature electrical measurements in a vacuum were carried out in a Lakeshore TTP-4 probe station with Keithley 4200 semiconductor analyzers. Measurements were taken in the vacuum chamber (~10^{-5} Torr) evacuated for more than 1 h. Liquid nitrogen was used to lower the device temperature to 78.4 K. The temperature of the devices was controlled by a temperature controller (Lake Shore, model 332).

Acknowledgment. We thank Alan Y. Liu for helpful discussions and acknowledge financial support by the National Science Foundation of China (nos. 20973007, 20973013, 51072004, 50821061, 20833001), the National Basic Research Program of China (nos. 2007CB936203, 2011CB921904, 2011CB933003), and SRF for ROCS, SEM.

Supporting Information Available: Experimental details and supplementary figures. This material is available free of charge *via* the Internet at http://pubs.acs.org.

REFERENCES AND NOTES

1. Novoselov, K. S.; Geim, A. K.; Morozov, S. V.; Jiang, D.; Zhang, Y.; Dubonos, S. V.; Grigorieva, I. V.; Firsov, A. A. Electric Field Effect in Atomically Thin Carbon Films. *Science* **2004**, *306*, 666–669.
2. Novoselov, K. S.; Geim, A. K.; Morozov, S. V.; Jiang, D.; Katsnelson, M. I.; Grigorieva, I. V.; Dubonos, S. V.; Firsov, A. A. Two-Dimensional Gas of Massless Dirac Fermions in Graphene. *Nature* **2005**, *438*, 197–200.
3. Bolotin, K. I.; Sikes, K. J.; Jiang, Z.; Klima, M.; Fudenberg, G.; Hone, J.; Kim, P.; Stormer, H. L. Ultrahigh Electron Mobility in Suspended Graphene. *Solid State Commun.* **2008**, *146*, 351–355.
4. Ohta, T.; Bostwick, A.; Seyller, T.; Horn, K.; Rotenberg, E. Controlling the Electronic Structure of Bilayer Graphene. *Science* **2006**, *313*, 951–954.
5. Barone, V.; Hod, O.; Scuseria, G. E. Electronic Structure and Stability of Semiconducting Graphene Nanoribbons. *Nano Lett.* **2006**, *6*, 2748–2754.
6. Boukhvalov, D. W.; Katsnelson, M. I. Chemical Functionalization of Graphene with Defects. *Nano Lett.* **2008**, *8*, 4373–4379.
7. Bekyarova, E.; Itkis, M. E.; Ramesh, P.; Berger, C.; Sprinkle, M.; de Heer, W. A.; Haddon, R. C. Chemical Modification of Epitaxial Graphene: Spontaneous Grafting of Aryl Groups. *J. Am. Chem. Soc.* **2009**, *131*, 1336–1337.
8. Elias, D. C.; Nair, R. R.; Mohiuddin, T. M. G.; Morozov, S. V.; Blake, P.; Halsall, M. P.; Ferrari, A. C.; Boukhvalov, D. W.; Katsnelson, M. I.; Geim, A. K.; *et al*. Control of Graphene's Properties by Reversible Hydrogenation: Evidence for Graphane. *Science* **2009**, *323*, 610–613.
9. Withers, F.; Dubois, M.; Savchenko, A. K. Electron Properties of Fluorinated Single-Layer Graphene Transistors. *Phys. Rev. B* **2010**, *82*, 073403.
10. Robinson, J. T.; Burgess, J. S.; Junkermeier, C. E.; Badescu, S. C.; Reinecke, T. L.; Perkins, F. K.; Zalalutdniov, M. K.; Baldwin, J. W.; Culbertson, J. C.; Sheehan, P. E.; *et al*. Properties of Fluorinated Graphene Films. *Nano Lett.* **2010**, *10*, 3001–3005.
11. Nair, R. R.; Ren, W. C.; Jalil, R.; Riaz, I.; Kravets, V. G.; Britnell, L.; Blake, P.; Schedin, F.; Mayorov, A. S.; Yuan, S. J.; *et al*. Fluorographene: a Two-Dimensional Counterpart of Teflon. *Small* **2010**, *6*, 2877–2843.
12. Wassei, J. K.; Cha, K. C.; Tung, V. C.; Yang, Y.; Kaner, R. B. The Effects of Thionyl Chloride on the Properties of Graphene and Graphene-Carbon Nanotube Composites. *J. Mater. Chem.* **2011**, *21*, 3391–3396.
13. Farmer, D. B.; Lin, Y. M.; Afzali-Ardakani, A.; Avouris, P. Behavior of a Chemically Doped Graphene Junction. *Appl. Phys. Lett.* **2009**, *94*, 213106.
14. Liu, H. T.; Ryu, S. M.; Chen, Z. Y.; Steigerwald, M. L.; Nuckolls, C.; Brus, L. E. Photochemical Reactivity of Graphene. *J. Am. Chem. Soc* . **2009**, *131*, 17099–17101.
15. Novoselov, K. S.; Jiang, D.; Schedin, F.; Booth, T. J.; Khotkevich, V. V.; Morozov, S. V.; Geim, A. K. Two-Dimensional Atomic Crystals. *Proc. Natl. Acad. Sci. U. S. A.* **2005**, *102*, 10451–10453.
16. Li, X. S.; Cai, W. W.; An, J. H.; Kim, S.; Nah, J.; Yang, D. X.; Piner, R.; Velamakanni, A.; Jung, I.; Tutuc, E.; *et al*. Large-Area Synthesis of High-Quality and Uniform Graphene Films on Copper Foils. *Science* **2009**, *324*, 1312–1314.
17. Li, X. S.; Cai, W. W.; Colombo, L.; Ruoff, R. S. Evolution of Graphene Growth on Ni and Cu by Carbon Isotope Labeling. *Nano Lett.* **2009**, *9*, 4268–4272.
18. Levendorf, M. P.; Ruiz-Vargas, C. S.; Garg, S.; Park, J. Transfer-Free Batch Fabrication of Single Layer Graphene Transistors. *Nano Lett.* **2009**, *9*, 4479–4483.
19. Yan, K.; Peng, H. L.; Zhou, Y.; Li, H.; Liu, Z. F. Formation of Bilayer Bernal Graphene: Layer-by-Layer Epitaxy *via* Chemical Vapor Deposition. *Nano Lett.* **2011**, *11*, 1106–1110.
20. Ishigami, M.; Chen, J. H.; Cullen, W. G.; Fuhrer, M. S.; Williams, E. D. Atomic Structure of Graphene on SiO_2. *Nano Lett.* **2007**, *7*, 1643–1648.
21. Roddaro, S.; Pingue, P.; Piazza, V.; Pellegrini, V.; Beltram, F. The Optical Visibility of Graphene: Interference Colors of Ultrathin Graphite on SiO_2. *Nano Lett.* **2007**, *7*, 2707–2710.
22. Ferrari, A. C.; Meyer, J. C.; Scardaci, V.; Casiraghi, C.; Lazzeri, M.; Mauri, F.; Piscanec, S.; Jiang, D.; Novoselov, K. S.; Roth, S.; *et al*. Raman Spectrum of Graphene and Graphene Layers. *Phys. Rev. Lett.* **2006**, *97*, 187401.
23. Kudin, K. N.; Ozbas, B.; Schniepp, H. C.; Prud'homme, R. K.; Aksay, I. A.; Car, R. Raman Spectra of Graphite Oxide and Functionalized Graphene Sheets. *Nano Lett.* **2008** *8*, 36–41.
24. Papirer, E.; Lacroix, R.; Donnet, J. B.; Nanse, G.; Fioux, P. XPS Study of the Halogenation of Carbon-Black 0.2. Chlorination. *Carbon* **1995**, *33*, 63–72.
25. Meyer, J. C.; Geim, A. K.; Katsnelson, M. I.; Novoselov, K. S.; Booth, T. J.; Roth, S. The Structure of Suspended Graphene Sheets. *Nature* **2007**, *446*, 60–63.
26. Kim, S.; Nah, J.; Jo, I.; Shahrjerdi, D.; Colombo, L.; Yao, Z.; Tutuc, E.; Banerjee, S. K. Realization of a High Mobility Dual-Gated Graphene Field-Effect Transistor with Al_2O_3 Dielectric. *Appl. Phys. Lett.* **2009**, *94*, 062107.
27. Tsui, D. C.; Allen, S. J. Mott-Anderson Localization in 2-Dimensional Band Tail of Si Inversion Layers. *Phys. Rev. Lett.* **1974**, *32*, 1200–1203.
28. Cheng, S. H.; Zou, K.; Okino, F.; Gutierrez, H. R.; Gupta, A.; Shen, N.; Eklund, P. C.; Sofo, J. O.; Zhu, J. Reversible Fluorination of Graphene: Evidence of a Two-Dimensional Wide Bandgap Semiconductor. *Phys. Rev. B* **2010**, *81*, 205435.